Mäkinen, Tero; Ovaska, Markus; Laurson, Lasse; Alava, Mikko

Portevin–Le Chatelier effect: modeling the deformation bands and stress-strain curves

Published in:
Materials Theory

DOI:
10.1186/s41313-022-00044-w

Published: 11/04/2022

Document Version
Publisher's PDF, also known as Version of record

Mäkinen *et al. Materials Theory* (2022) 6:15
https://doi.org/10.1186/s41313-022-00044-w

Materials Theory

ORIGINAL ARTICLE Open Access

Portevin–Le Chatelier effect: modeling the deformation bands and stress-strain curves

Tero Mäkinen[1,2*], Markus Ovaska[1], Lasse Laurson[3] and Mikko J. Alava[1,2]

*Correspondence:
tero.j.makinen@aalto.fi
[1]Department of Applied Physics, Aalto University, P.O. Box 11100, 00076 Aalto Espoo, Finland
Full list of author information is available at the end of the article

Abstract

In the Portevin–Le Chatelier (PLC) effect sample plastic deformation takes place via localized bands. We present a model to account for band dynamics and the variability the bands exhibit. The approach is tuned to account for strain hardening and the strain-rate dependence for the case of so-called type A (propagating) bands. The main experimental features of the fluctuations are a reduction with strain and increase with the strain rate which is reproduced by a model of plastic deformation with Dynamic Strain Aging, including disorder as a key parameter. Extensions are discussed as are the short-comings in reproducing detailed avalanche statistics.

Keywords: Plastic instability, Deformation bands, Dynamic strain aging

Introduction

Complexity in materials deformation is both important for engineering and of interest for the basic physics implied. Metals when loaded beyond the elastic regime yield and the plastic deformation prior to failure is now known to exhibit very complex properties on various scales in time and space (Zaiser 2006; Papanikolaou et al. 2018; Alava et al. 2014). The localization phenomena in the deformation of a specimen in plasticity are an example, and shear bands appear in various scenarios of which we here study the Portevin–Le Chatelier (Le Chatelier 1909; Portevin and Le Chatelier 1923) (PLC) effect.

The PLC effect implies the creation of deformation bands in a sample (Fig. 1) when loaded beyond the yield point. Recall that such bands nucleate, and may or may not propagate depending on the class of PLC instablity present (type A denotes propagating bands, type B bands that propagate in an intermittent, 'hopping' fashion, and type C non-propagating bands). This kind of phenomena – related to negative Strain-Rate Sensitivity (Wilcox and Rosenfield 1966; Xu et al. 2022) (SRS) – arises as a strain rate dependent phenomenon; moreover its character and presence are dependent on the temperature. The PLC effect is attributed to Dynamic Strain Aging (Cottrell and Bilby 1949; Zaiser and Hähner 1997) (DSA), and the crucial physics is in the interaction of the dislocations as the fundamental source of plastic deformation with the solute atoms in the metal alloy

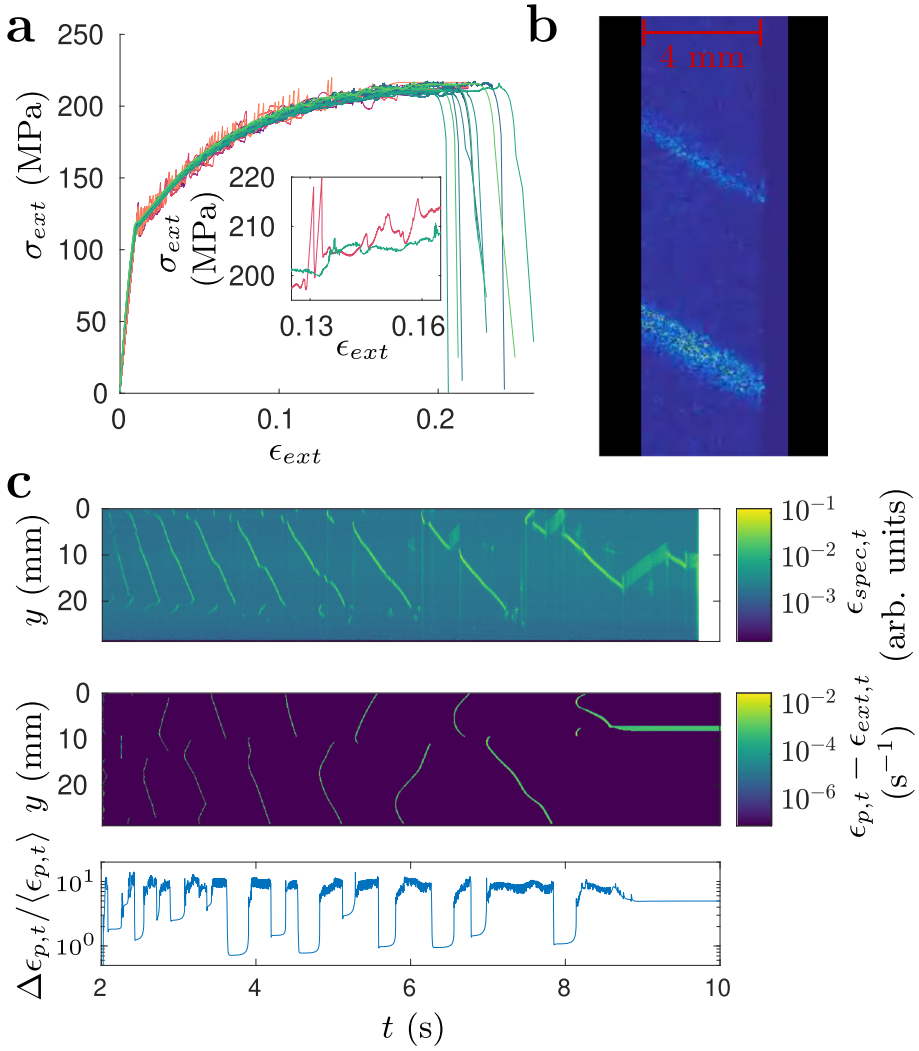

Fig. 1 **a** The stress-strain curves showing the responses from experiments (green) and simulations (red) superimposed. The Inset shows the stress serrations in magnified view. **b** The raw subtracted speckle images showing two simultaneous PLC bands. **c** Two strain rate maps showing the experimental effective strain rate $\epsilon_{spec,t}$ (top) for one band inclination and for comparison the difference of plastic strain rate $\epsilon_{p,t}$ and applied strain rate $\epsilon_{ext,t}$ during a simulation done with the same strain rate. Below the relative standard deviation of the plastic strain rate in the simulation

(McCormick 1972; Van den Beukel 1975; Zhao et al. 2020). On the mesoscopic level, theories of increasing complexity have been proposed such that they would account for the necessary dislocation physics: elementary classes of immobile and "aging", solute bound dislocations, and mobile ones producing plastic deformation. Such models and a multitude of experiments have been recently introduced to explore the physics of the PLC effect: phases in the band nucleation (Shabadi et al. 2004a; Tong et al. 2005; Halim et al. 2007; Casarotto et al. 2009; Klusemann et al. 2015) and dynamics including serrations in the stress-strain curves (Lebyodkin et al. 1996; Rajesh and Ananthakrishna 2000; Bharathi et al. 2001; Chihab and Fressengeas 2003; Lebyodkin and Estrin 2005; Chatterjee et al. 2008; Kumar et al. 2015), Acoustic Emission (Lebyodkin and Lebedkina 2021; Chmelík et al. 2002; Chmelík et al. 2007; Louche et al. 2008; Shashkov et al. 2012; Lebyodkin et al.

2013; Kumar et al. 2015) from the PLC effect and so forth. We have recently shown how the shear bands' dynamics and their fluctuations reflect the collective dynamics of mobile dislocation assemblies (Mäkinen et al. 2020), in the case of a commercial Al alloy which produces type A and B bands in the PLC regime (Dablij and Zeghloul 1997). The model introduced by us considers PLC bands as point particles moving in a disordered landscape ("pinning") under a driving force and coupled to the system ("average deformation rate") such that eg. the strain rate of an experiment can be accounted for as well as the strain hardening during the stress-strain curve.

Here, we take a different look by abstaining from the coarse-graining of the aforementioned model. The main question is how one can reproduce such experiments with a model that accounts for the aging behavior of dislocation assemblies (as we shall see below, understood still after an averaging step to reduce the dimensionality). This could be understood as, how do the PLC band velocities reflect the collective nature of the dislocation dynamics? One common observation has been the decrease of the band velocity $\overline{v_b}$ with applied strain ϵ_{ext} (Ranc and Wagner 2008; Chen et al. 2007; Benallal et al. 2008a; Benallal et al. 2008b; Shabadi et al. 2004a; Jiang et al. 2007; Jiang et al. 2005; Shabadi et al. 2004b; Klose et al. 2004; Louche et al. 2008; Ait-Amokhtar et al. 2006; Dahdouh et al. 2021) including Al alloys similar to our original study. Another relation is a power-law relation of the band velocity to the applied strain rate $\overline{v_b} \propto \epsilon^s_{ext,t}$. This has been observed in many different alloys with exponents in the proximity of unity (Ait-Amokhtar et al. 2006; Ziegenbein et al. 2000; Hähner et al. 2001; Klose et al. 2004; Benallal et al. 2008b; Lebedkina et al. 2009; Jiang et al. 2007).

Given the complexity of the PLC phenomena a number of earlier models (Ananthakrishna 2007) have been proposed. They range from reproducing the stress-strain curves without considering the band propagation (the Kubin–Estrin model (Kubin and Estrin 1990; Lebyodkin et al. 1995)) to models being exploited on macroscopic Finite Element Simulations (Zhang et al. 2001; Kok et al. 2003; Lasko et al. 2005; Benallal et al. 2008a; Klusemann et al. 2015; Ren et al. 2017; Ren et al. 2021). On the mesoscopic level we consider here one has to deal with local, coarse-grained dislocation densities and some models are based on directly modeling the DSA mechanism (the Hähner et al. (2002) or Jiang et al. (2007) models) but there is also the Ananthakrishna model (Bharathi et al. 2003) which is based on directly modeling the interactions between dislocations and divides them into three types: the mobile ones, the immobile ones and the Cottrell ones which accumulate a solute cloud. In the following we concentrate on the HR model, and on how it can be made to reproduce experimental observations. The rest of the paper is structured so that in Model and data section, we overview the data we compared the model with (following Ref. Mäkinen et al. (2020)) and how and why the original HR model has been developed. In Results section, we look at band statistics from the model presented, at various strain rates and as observed over the stress-strain curve, and compare with experiment. Section finishes with an outlook and discussion.

Model and data

Experiments

We briefly repeat the details of the data presented in Ref. Mäkinen et al. (2020). The laser speckle technique (Shabadi et al. 2004a) was used to observe the bands in a commercial

aluminum alloy AW-5754 sample with the dimensions 28 mm $\times$4 mm $\times$0.5 mm for the gauge volume.

The samples were tensile loaded with Instron ElectroPuls E1000 using an Instron Dynacell load cell with a constant displacement rate. The stress and strain were recorded with an acquisition rate of 500 Hz. The speckle pattern was recorded with a acquisition rates varying around 0.5-2.0 kHz and finally processed to a 1D projection (Fig. 1). Subtraction of two speckle images shows the differences on the sample surface and as this difference is an indication (but not a measure) of high strain rates, we denote it (after projection) as the effective strain rate $\epsilon_{spec,t}$. The maximum value of $\epsilon_{spec,t}$ around the visible band corresponds to the leading edge of the band and this slightly noisy signal was smoothed using a moving average with a 15-60 ms window. The initial and final transients of the velocity can be quite large and therefore the average velocity $\overline{v_b}$ was calculated from the middle 50% of the velocity signal. The PLC effect in the experiments and in the model – due to the disorder added – exhibit memory effects as the Fig. 1c also implies such as typical locations at which a band nucleates or stops in each sample. We do not investigate this here in any detail but an average over all the experiments tells that the nucleation is spread rather homogeneously, and does not happen just at the specimen endpoints.

Model

A one dimensional model based on work by Hähner et al. (2002) (HR) has been developed here. The HR theory is based on a traditional DSA mechanism and the evolution equations read here

$$\epsilon_{p,t}(y) = \nu\Omega \exp\left(-\frac{G_0 + G^{ag}(y)}{k_B T} + \frac{\sigma_{ext} - \sigma_{int}(y)}{S_0}\right) \tag{1}$$

$$G^{ag}_{,t}(y) = DG^{ag}_{,yy}(y) + \eta\left[G^{ag}_{\infty} - G^{ag}(y)\right] - \frac{G^{ag}(y)}{\Omega}\epsilon_{p,t}(y) \tag{2}$$

$$\sigma_{int,t}(y) = h_0 \exp\left[-h_{exp}\epsilon_p(y)\right]\epsilon_{p,t}(y) \tag{3}$$

where ϵ_p is the plastic strain (so that $\epsilon_{ext} = \epsilon_p + \epsilon_e$), ν the attempt frequency of thermal activation, Ω the elementary plastic strain, G_0 the activation enthalpy without aging, G^{ag} the effect of aging on the activation enthalpy, k_B the Boltzmann constant, T the absolute temperature, σ_{ext} the applied external stress (flow stress), σ_{int} the internal stress (athermal back stress), S_0 the instantaneous SRS of the flow stress, D the diffusion coefficient, η the aging rate, G^{ag}_{∞} the saturation value of the additional activation enthalpy, and y the spatial coordinate along the sample. This approach reproduces traveling waves or bands. To account for the hardening and to match with the experimental behavior (stress-strain curve) the equation for the internal stress uses the Voce hardening model (Voce 1948) with hardening parameters h_0 and h_{exp} as the first modification of the HR model. As can be seen in Fig. 1a the stress responses from experiments and simulations have almost superimposed curves. Secondly instead of a global average over the sample the hardening (in Eq. 3) was considered as a local memory effect with the hardening coefficient

$$h = h_0 \exp(-h_{exp}\epsilon_p). \tag{4}$$

This was done to reproduce the observed higher fluctuations in the band velocity and the hardening behavior can be seen in Fig. 2a.

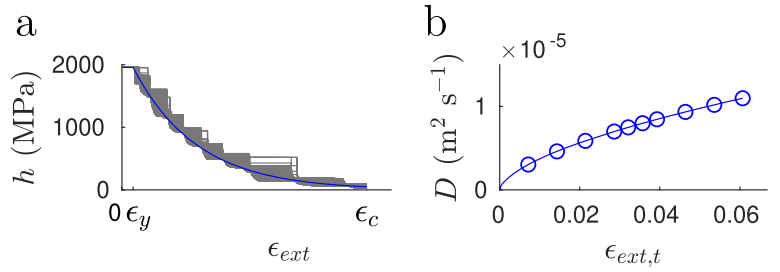

Fig. 2 **a** The strain evolution of the expected average hardening coefficient $\langle h \rangle$ (blue) and the local hardening parameter values from one simulation (grey). The drops in the local hardening coefficient signify increases in the local plastic strain due to passing of bands. **b** The strain rate dependence of the parameter $D = D_0 \epsilon_{ext,t}^{\gamma}$

To reproduce the band velocity variation and its dependence on the applied strain rate we introduced a random initial condition, by a Gaussian distribution of the plastic strain rate around a mean $\epsilon_{p,t}^0$ and with a standard deviation $\Delta\epsilon_{p,t}^0$, together with fully aged dislocations $G_0^{ag} = G_\infty^{ag}$ and an initial external stress σ_{ext}^0. Finally these equations are coupled to the constant strain rate machine equation

$$\sigma_{ext,t}(y) = E^\star \left[\epsilon_{ext,t} - \frac{1}{L} \int_0^L \epsilon_{p,t}(y)\, \mathrm{d}y \right] \tag{5}$$

where $E^\star$ is the combined modulus of the sample and the machine and L the sample length.

The diffusive spatial coupling in Eq. 2 has been motivated by the long-range dislocation correlations present in the system (Hähner et al. 2002), which would give the value of the (pseudo)diffusion coefficient as $D \approx \frac{\mu}{S_0} \beta_g G_{min}^{ag} k_B T \epsilon_{b,t} s^2$ where μ is the shear modulus, β_g a geometry factor, G_{min}^{ag} the minimum value of G^{ag}, $\epsilon_{b,t}$ the band strain rate, and s the specimen thickness. This parameter controls the band velocities and to reproduce the large spread in those we have introduced a strain rate dependent D with $D = D_0 \epsilon_{ext,t}^{\gamma}$ (which is seen in Fig. 2b). If the band velocity evolves as $\langle \overline{v_b} \rangle \propto \epsilon_{ext,t}^s$, this would give $D \propto \langle \overline{v_b} \rangle^{\gamma/s}$. As shown above, $D \propto \epsilon_{b,t}$, and the band strain has been shown to vary e.g. with the strain rate (Kang et al. 2012) and the stress serration amplitude (Cai et al. 2017) so we find this strain rate dependent D a reasonable modification. The Inset in Fig. 3 shows the average band velocities with a constant D and the variation is clearly smaller.

In the fitting of the parameters we can set nine of them directly based on the sample dimensions (L) and the general shape of the experimental stress-strain curve (σ_{ext}^0, $E^\star$, $\langle \epsilon_y \rangle$, $\epsilon_{p,t}^0$ and S_0 based on the behavior before yielding, and $\langle \epsilon_c \rangle$, h_0 and h_{exp} based on the hardening behavior) and the tenth by starting the simulation with fully aged dislocations $G_0^{ag} = G_\infty^{ag}$. This leaves G_∞^{ag}, $\Delta\epsilon_{p,t}^0$, η, Ω and D as free parameters. We first carefully choose G_∞^{ag}, η, and Ω so that the strain rate ranges match the type A to type B band transition in the experiments (as we see some type B bands with lower strain rates although they are excluded from our analysis) and the PLC instability is present in the whole tested strain rate region (utilizing the linear stability analysis presented in Ref. Hähner et al. (2002)) which results in our fairly high G_∞^{ag}. The model is sensitive to changes in these parameter values, especially close to the type A to B transition. After that the value of D was set so that the average velocities were close to the experimental values and a

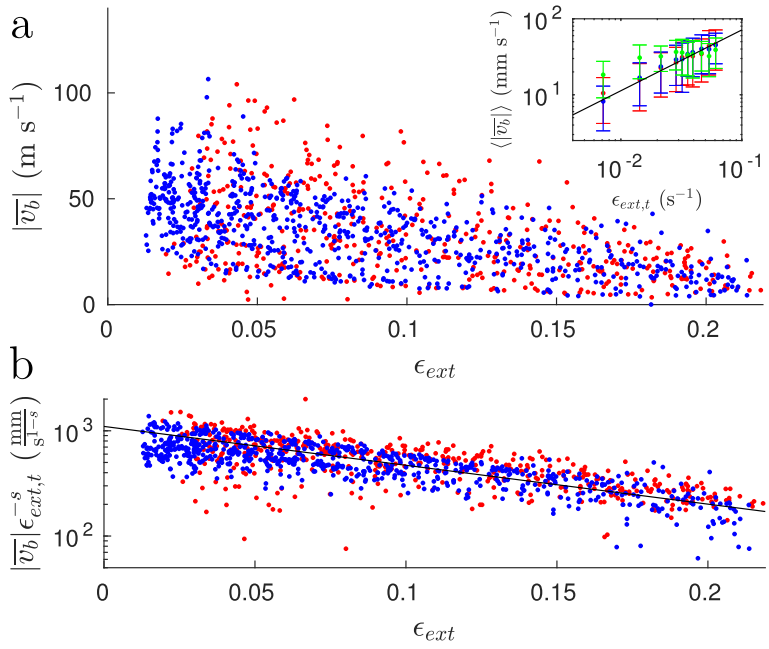

Fig. 3 **a** The behavior of mean band velocities with external strain in experiments (red) and simulations (blue). The Inset shows the mean band velocity from experiments (red) and simulations (blue) as a function of the strain rate and behavior of the simulations (green) with a constant $D = 7 \cdot 10^{-6}$ m^2/s. The straight line is a power-law fit $\epsilon_{ext,t}^{0.8}$. **b** The scaled velocities from experiments (red) and simulations (blue). The black line is an exponential fit exp $(-8.5 \cdot \epsilon_{ext})$

power-law (seen in Fig. 2b) was fitted. Finally $\Delta\epsilon_{p,t}^0$ was set so that it best reproduces the experimentally seen average fluctuations. The parameter values are in Table 1. The sample was discretized into 200 sections to match the spatial resolution of the experiments and the evolution equations were numerically solved using the adaptive Dormand–Prince RK5(4)7M method (Dormand and Prince 1986). Analogously to the experiments the band movement was tracked by computing the strain rate maps and tracking the band front.

Table 1 Parameter values for the model

Parameter	Value
G_0^{ag}	$15k_BT$
G_∞^{ag}	$15k_BT$
$\epsilon_{p,t}^0$	$2.8 \cdot 10^{-22}$ s^{-1}
$\Delta\epsilon_{p,t}^0$	$0.1 \cdot \epsilon_{p,t}^0$ s^{-1}
σ_{ext}^0	2.0 MPa
S_0	3.0 MPa
$E^\star$	11.4 GPa
L	28 mm
η	50 s^{-1}
Ω	$1.2 \cdot 10^{-4}$
D_0	$5.9 \cdot 10^{-5}$ m^2 s$^{\gamma-1}$
γ	0.6
h_0	1958 MPa
h_{exp}	17.62
$\langle\epsilon_y\rangle$	$1.0 \cdot 10^{-2}$
$\langle\epsilon_c\rangle$	$2.19 \cdot 10^{-1}$

Results

The general mechanical behavior of the samples in the simulations is shown in Fig. 1a,c. The model reproduces the experiments though the large serrations are around 10 MPa larger in the simulations. This can be explained by the delayed response of the experimental setup to a spike in the strain rate (the constant strain rate is achieved by controlling the stress rate based on the strain rate observed). The (effective) strain rate maps show matching behavior and band velocities for an experiment and a simulation done with the same strain rate. The band width w_b was 0.9 $\pm$0.1 mm in experiments, which is close to the sample thickness, and 0.3 $\pm$0.1 mm in simulations. The small fluctuations in the band width did not seem correlated with the velocity fluctuations and were not considered in our analysis.

The velocity trends as a function of strain rate and over the stress-strain curve are illustrated in Fig. 3 and in the experiments the average band velocity behaves roughly as $|\overline{v_b}| \propto \exp(-8.5 \cdot \epsilon_{ext})$ so a decrease in the average velocity of single bands during the tests is evident. There are also many slow bands in the beginning of the test. The effect of the strain rate follows $\langle|\overline{v_b}|\rangle \propto \dot{\epsilon}_{ext,t}^{0.8}$ (Fig. 3 and Inset) and with the power-law rate dependence in the D parameter these are reproduced in the simulations. We note that the small differences in these velocity trends compared to Ref. Mäkinen et al. (2020) are due to the difference in the determination of the average velocity (here we ignore the transients).

Categorizing the fluctuations as the standard deviation of the velocity

$$\overline{\Delta v_b} = \sqrt{\overline{(v_b - \overline{v_b})^2}} \tag{6}$$

and ignoring the transients by considering only the middle half of the signal produces the results seen in Fig. 4. A decreasing spread of the velocity fluctuations can be seen during the experiment. This trend diminishes when considering the relative velocity fluctuations $\frac{\Delta v_b}{\overline{v_b}}$ as seen in Fig. 4b,d which means that the fluctuations scale with the band velocity. The same scaling can be seen in the average fluctuations as a function of the strain rate as the fluctuations increase with strain rate but the relative fluctuations stay roughly constant. This behavior is found from the model but towards the end of a test the fluctuations start increasing which can be seen even better in the relative fluctuations. This could be as such due to the sample getting closer to failure and effects outside of our model (for example necking) having an effect. However, our earlier comparison with the Alessandro–Beatrice–Bertotti–Montorsi (ABBM) model (Alessandro et al. 1990) reproduces the statistics better as we discuss below. This shows in simple terms that the description of the effective disorder the band encounters and of the band interaction with that is crucial and is not completely caught by the current model.

We finally present in Fig. 5 a comparison of the experimental data with the current model and the ABBM one for the avalanche sizes or distances of band propagation S. The ABBM approach has a formal expression for $P(S)$ which nicely reproduces the experiment while the Hähner-Rizzi model variant nevertheless produces a wide distribution which is also surprisingly close to the experimental one.

There are naturally other quantities one could compare between the experiments and the model, e.g. the stress drops, the velocity distribution, and the critical strain for the first band occurrence. There is a clear difference in the stress drops, as seen in Fig. 1 and the related discussion regarding the stress-strain curves. In terms of the velocity distribution

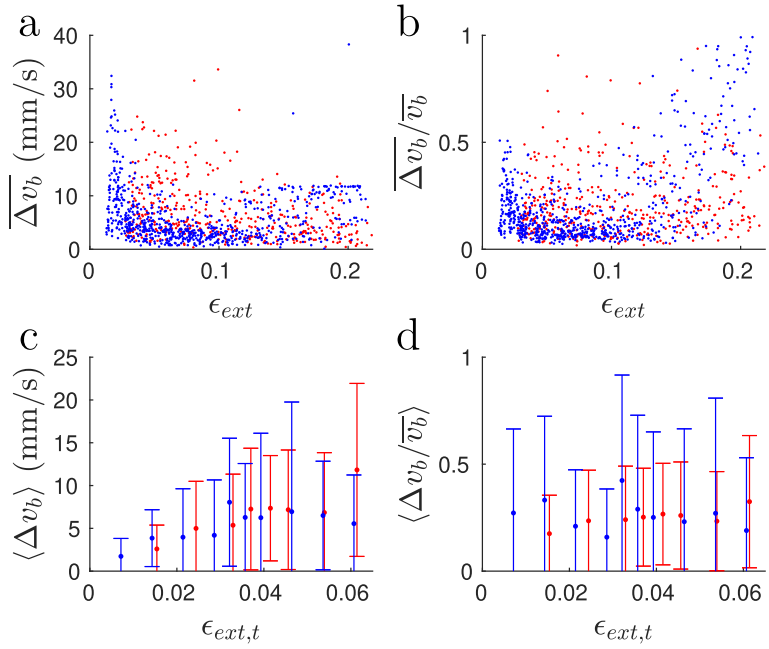

Fig. 4 **a** Band velocity fluctuations as a function of strain for experiments (red) and simulations (blue). **b** Same as a but for relative velocity fluctuations. **c** The average velocity fluctuations as a function of strain rate for experiments (red) and simulations (blue). **d** Same as c but for average relative velocity fluctuations

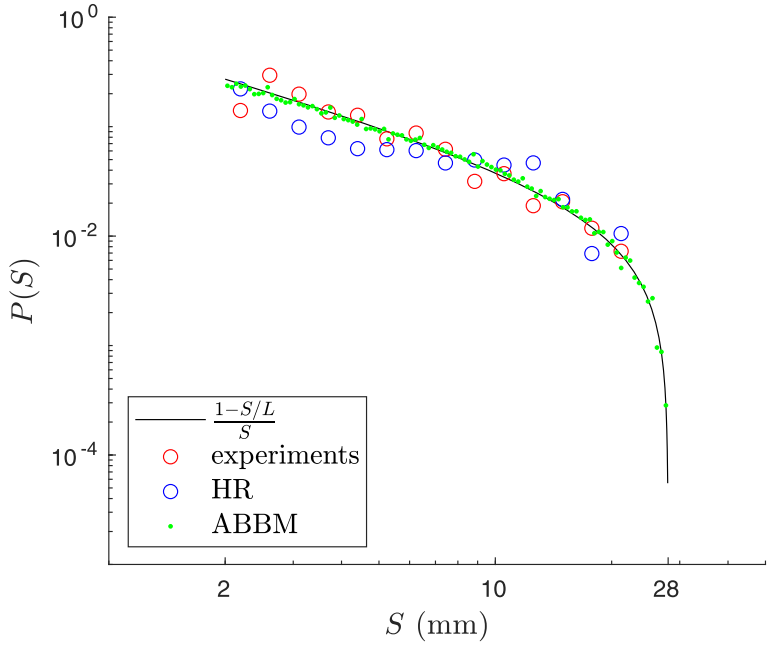

Fig. 5 The distribution of band propagation distances (or avalanche sizes) in the experiments (red) in the Hähner–Rizzi model simulations (blue), and the ABBM model simulations (green). The black line represents the expected form of the distribution $P(S) = A(1 - \frac{S}{L})/S$ where $A = \left(\frac{S_0}{L} + \ln \frac{L}{L_0} - 1\right)^{-1}$ and $S_0 = 2$ mm

we have here only looked at the average and the fluctuations of the middle (stable) part of the velocity profiles. The transient parts of the profiles differ slightly between the simulations and experiments (full experimental velocity distribution is studied in Ref. Mäkinen et al. (2020)). One can also directly see from Fig. 3 that the strain of the first band occurrence is higher in the experiments. This critical strain increases slightly with strain rate but as we are only considering the type A band regime we do not see a large increase with lower strain rates.

Conclusions

We have studied the statistics of the PLC plastic deformation bands with the help of a 1D model of DSA. The actual experimental data exhibits trends with loading rate and with the hardening during straining and we tune the model to be able to have bands that are close to the experimental ones and to be able to mimic the stress-strain curves. The crucial ideas needed to get this match are the locally varying nature of the driving force, accounting for the locally varying activation enthalpy and spatially varying hardening and the strain-rate dependent diffusion terms for the activation enthalpy.

Common in this approach compared to the ABBM approach is that for the band velocity profiles we argue that the band velocity is unique for each band and arises from the local disorder at the time of band nucleation. In the context of our model this stems from the initial disorder of the system. A key component in the evolution of the system is the hardening which here is modeled using the Voce model. To summarize, this approach is a one-dimensional reduced description of a whole sample (whereas ABBM-style avalanche models just consider the avalanches/bands after they have been nucleated).

The success of the ABBM approach in describing the details of the band velocity profiles and their evolution sets a clear constraint to further model development. More complex models describing the PLC effect, including for example the stress-strain behavior and higher dimensionality, should reproduce this ABBM-style velocity behavior, or in other words, reduce to a model reproducing this behavior..

More work is needed in explaining the large variability in the band velocity: this is an effect that is present in the PLC generally, and clearly must depend quantitatively on the material composition (and processing). This model could also be studied to check how it reproduces the physics in the type B band regime, where bands propagate in an intermittent, 'hopping' fashion. For all models involving a dimensional reduction the question remains what details they actually miss from the 2D or 3D nature of the PLC effect.

Acknowledgements
Aalto Science IT project is acknowledged for computational resources.

Authors' contributions
TM and MO performed the experiments, and TM analyzed the data and performed the simulations. TM, LL, and MJA wrote the manuscript. All authors read and approved the final manuscript.

Funding
We acknowledge the financial support from the Academy of Finland through the Center of Excellence program (Project No. 251748) and the Academy Project COPLAST (LL, Project No. 322405). MJA and TM acknowledge support from the European Union Horizon 2020 research and innovation program under grant agreement no. 857470 and from the European Regional Development Fund via the Foundation for Polish Science International Research Agenda PLUS program grant No. MAB PLUS/2018/8. TM also acknowledges funding from The Finnish Foundation for Technology Promotion.

Availability of data and materials
The datasets used and analysed during the current study are available from the corresponding author on reasonable request.

Declarations

Competing interests
The authors declare that they have no competing interests.

Author details
[1]Department of Applied Physics, Aalto University, P.O. Box 11100, 00076 Aalto Espoo, Finland. [2]NOMATEN Centre of Excellence, National Centre for Nuclear Research, ul. A. Soltana 7, 05-400 Swierk/Otwock, Poland. [3]Computational Physics Laboratory, Tampere University, P.O. Box 692, FI-33014 Tampere, Finland.

Received: 11 November 2021 Accepted: 28 March 2022
Published online: 11 April 2022

References
H. Ait-Amokhtar, P. Vacher, S. Boudrahem, Kinematics fields and spatial activity of Portevin-Le Chatelier bands using the digital image correlation method. Acta Mater. **54**(16), 4365–4371 (2006). https://doi.org/10.1016/j.actamat.2006.05.028

M. J. Alava, L. Laurson, S. Zapperi, Crackling noise in plasticity. Eur. Phys. J. Spec. Top. **223**(11), 2353–2367 (2014). https://doi.org/10.1140/epjst/e2014-02269-8

B. Alessandro, C. Beatrice, G. Bertotti, A. Montorsi, Domain-wall dynamics and Barkhausen effect in metallic ferromagnetic materials. I. Theory. J. Appl. Phys. **68**(6), 2901–2907 (1990)

G. Ananthakrishna, Current theoretical approaches to collective behavior of dislocations. Phys. Rep. **440**(4-6), 113–259 (2007)

A. Benallal, T. Berstad, T. Børvik, O. S. Hopperstad, I. Koutiri, R. Nogueira de Codes, An experimental and numerical investigation of the behaviour of AA5083 aluminium alloy in presence of the Portevin-Le Chatelier effect. Int. J. Plas. **24**(10), 1916–1945 (2008a). https://doi.org/10.1016/j.ijplas.2008.03.008

A. Benallal, T. Berstad, T. Børvik, O. S. Hopperstad, R. Nogueira De Codes, Effects of strain rate on the characteristics of PLC deformation bands for AA5083-H116 aluminium alloy. Philosoph. Mag. **88**(28-29), 3311–3338 (2008b). https://doi.org/10.1080/14786430802468223

M. S. Bharathi, M. Lebyodkin, G. Ananthakrishna, C. Fressengeas, L. P. Kubin, Multifractal burst in the spatiotemporal dynamics of jerky flow. Phys. Rev. Lett. **87**(16), 165508 (2001)

M. S. Bharathi, S. Rajesh, G. Ananthakrishna, A dynamical model for the Portevin–Le Chatelier bands. Scripta Mater. **48**(9), 1355–1360 (2003). https://doi.org/10.1016/S1359-6462(02)00653-X

Y. Cai, S. Yang, S. Fu, D. Zhang, Q. Zhang, Investigation of Portevin–Le Chatelier band strain and elastic shrinkage in Al-based alloys associated with Mg contents. J. Mater. Sci. Technol. **33**(6), 580–586 (2017)

L. Casarotto, H. Dierke, R. Tutsch, H. Neuhäuser, On nucleation and propagation of PLC bands in an Al-3Mg alloy. Mater. Sci. Eng. A. **527**(1-2), 132–140 (2009). https://doi.org/10.1016/j.msea.2009.07.043

A. Chatterjee, A. Sarkar, S. Bhattacharya, P. Mukherjee, N. Gayathri, P. Barat, Markov property of continuous dislocation band propagation. Phys. Lett. A. **372**(22), 4016–4020 (2008). https://doi.org/10.1016/j.physleta.2008.03.013

L. Chen, H.-S. Kim, S.-K. Kim, B. C. De Cooman, Localized Deformation due to Portevin–LeChatelier Effect in 18Mn–0.6C TWIP Austenitic Steel. ISIJ Int. **47**(12), 1804–1812 (2007). https://doi.org/10.2355/isijinternational.47.1804

K. Chihab, C. Fressengeas, Time distribution of stress drops, critical strain and crossover in the dynamics of jerky flow. Mater. Sci. Eng. A. **356**(1-2), 102–107 (2003). https://doi.org/10.1016/S0921-5093(03)00141-2

F. Chmelík, F. B. Klose, H. Dierke, J. Šachl, H. Neuhäuser, P. Lukáč, Investigating the Portevin-Le Châtelier effect in strain rate and stress rate controlled tests by the acoustic emission and laser extensometry techniques. Mater. Sci. Eng. A. **462**(1-2), 53–60 (2007). https://doi.org/10.1016/j.msea.2006.01.169

F. Chmelík, A. Ziegenbein, H. Neuhäuser, P. Lukáč, Investigating the Portevin–Le Châtelier effect by the acoustic emission and laser extensometry techniques. Mater. Sci. Eng. A. **324**(1-2), 200–207 (2002). https://doi.org/10.1016/S0921-5093(01)01312-0

A. H. Cottrell, B. A. Bilby, Dislocation theory of yielding and strain ageing of iron. Proc. Phys. Soc. A. **62**(1), 49–62 (1949)

M. Dablij, A. Zeghloul, Portevin-Le Chatelier plastic instabilities: Characteristics of deformation bands. Mater. Sci. Eng. A. **237**(1), 1–5 (1997). https://doi.org/10.1016/S0921-5093(97)00101-9

S. Dahdouh, M. Mehenni, H. Ait-Amokhtar, Kinetics of formation and propagation of type A Portevin-Le Chatelier bands in the presence of a small circular hole. J. Alloys Compd. **885**, 160982 (2021)

J. R. Dormand, P. J. Prince, A reconsideration of some embedded Runge–Kutta formulae. J. Comp. Appl. Math. **15**(2), 203–211 (1986). https://doi.org/10.1016/0377-0427(86)90027-0

P. Hähner, A. Ziegenbein, H. Neuhäuser, Observation and modelling of propagating Portevin-Le Châtelier deformation bands in Cu-15at.% Al polycrystals. Philosoph. Mag. A. **81**(6), 1633–1649 (2001). https://doi.org/10.1080/01418610108214367

P. Hähner, A. Ziegenbein, E. Rizzi, H. Neuhäuser, Spatiotemporal analysis of Portevin-Le Châtelier deformation bands: Theory, simulation, and experiment. Phys. Rev. B. **65**(13), 134109 (2002). https://doi.org/10.1103/PhysRevB.65.134109

H. Halim, D. S. Wilkinson, M. Niewczas, The Portevin-Le Chatelier (PLC) effect and shear band formation in an AA5754 alloy. Acta Mater. **55**(12), 4151–4160 (2007). https://doi.org/10.1016/j.actamat.2007.03.007

H. Jiang, Q. Zhang, X. Chen, Z. Chen, Z. Jiang, X. Wu, J. Fan, Three types of Portevin-Le Chatelier effects: Experiment and modelling. Acta Mater. **55**(7), 2219–2228 (2007). https://doi.org/10.1016/j.actamat.2006.10.029

H. F. Jiang, Q. C. Zhang, Z. Y. Jiang, Z. J. Chen, X. P. Wu, Investigation of kinematics of the Portevin-Le Chatelier deformation bands with dynamic digital speckle pattern interferometry. Chin. Phys. Lett. **22**(1), 99–102 (2005). https://doi.org/10.1088/0256-307X/22/1/028

H. Jiang, Q. Zhang, Z. Jiang, X. Wu, Experimental investigations on kinetics of Portevin-Le Chatelier effect in Al-4 wt.%Cu alloys. J. Alloys Compd. **428**(1-2), 151–156 (2007). https://doi.org/10.1016/j.jallcom.2006.03.062

J. Kang, R. K. Mishra, D. S. Wilkinson, O. S. Hopperstad, Effect of Mg content on Portevin–Le Chatelier band strain in Al-Mg sheet alloys. Philos. Mag. Lett. **92**(11), 647–655 (2012)
F. B. Klose, F. Hagemann, P. Hähner, H. Neuhäuser, Investigation of the Portevin-LeChâtelier effect in Al-3wt.%Mg alloys by strain-rate and stress-rate controlled tensile tests. Mater. Sci. Eng. A. **387-389**(1-2 SPEC. ISS), 93–97 (2004). https://doi.org/10.1016/j.msea.2004.01.062
B. Klusemann, G. Fischer, T. Böhlke, B. Svendsen, Thermomechanical characterization of Portevin-Le Châtelier bands in AlMg3 (AA5754) and modeling based on a modified Estrin–McCormick approach. Int. J. Plas. **67**, 192–216 (2015). https://doi.org/10.1016/j.ijplas.2014.10.011
S. Kok, M. Bharathi, A. Beaudoin, C. Fressengeas, G. Ananthakrishna, L. Kubin, M. Lebyodkin, Spatial coupling in jerky flow using polycrystal plasticity. Acta Mater. **51**(13), 3651–3662 (2003)
L. Kubin, Y. Estrin, Evolution of dislocation densities and the critical conditions for the Portevin-Le Chatelier effect. Acta Metall. Mater. **38**(5), 697–708 (1990)
J. Kumar, R. Sarmah, G. Ananthakrishna, General framework for acoustic emission during plastic deformation. Phys. Rev. B. **92**(14), 144109 (2015). https://doi.org/10.1103/PhysRevB.92.144109
G. Lasko, P. Hähner, S. Schmauder, Finite element simulation of the Portevin-Le Chatelier effect. Modell. Simul. Mater. Sci. Eng. **13**(5), 645–656 (2005). https://doi.org/10.1088/0965-0393/13/5/001
A. Le Chatelier, Influence du temps et de la température sur les essais au choc. Rev. Métall. **6**(8), 914–917 (1909)
T. A. Lebedkina, M. A. Lebyodkin, J. P. Chateau, A. Jacques, S. Allain, On the mechanism of unstable plastic flow in an austenitic FeMnC TWIP steel. Mater. Sci. Eng. A. **519**(1-2), 147–154 (2009). https://doi.org/10.1016/j.msea.2009.04.067
M. A. Lebyodkin, Y. Brechet, Y. Estrin, L. P. Kubin, Statistics of the Slip Events in the Portevin-Le Chatelier Effect. Phys. Rev. Lett. **74**(23), 4758–4761 (1995)
M. Lebyodkin, Y. Brechet, Y. Estrin, L. Kubin, Statistical behaviour and strain localization patterns in the Portevin-Le Chatelier effect. Acta Mater. **44**(11), 4531–4541 (1996). https://doi.org/10.1016/1359-6454(96)00076-6
M. A. Lebyodkin, Y. Estrin, Multifractal analysis of the Portevin–Le Chatelier effect: General approach and application to AlMg and AlMg/Al_2O_3 alloys. Acta Mater. **53**(12), 3403–3413 (2005)
M. A. Lebyodkin, T. A. Lebedkina, The Portevin-Le Chatelier effect and beyond. arXiv preprint arXiv:2104.07018 (2021). https://doi.org/10.48550/arXiv.2104.07018
M. A. Lebyodkin, I. V. Shashkov, T. A. Lebedkina, K. Mathis, P. Dobron, F. Chmelik, Role of superposition of dislocation avalanches in the statistics of acoustic emission during plastic deformation. Phys. Rev. E. **88**(4), 042402 (2013). https://doi.org/10.1103/PhysRevE.88.042402
H. Louche, K. Bouabdallah, P. Vacher, T. Coudert, P. Balland, Kinematic fields and acoustic emission observations associated with the Portevin Le Châtelier effect on an Al-Mg alloy. Exp. Mech. **48**(6), 741–751 (2008). https://doi.org/10.1007/s11340-008-9125-5
T. Mäkinen, P. Karppinen, M. Ovaska, L. Laurson, M. J. Alava, Propagating bands of plastic deformation in a metal alloy as critical avalanches. Sci. Adv. **6**(41), 7350 (2020)
P. G. McCormick, A model for the Portevin-Le Chatelier effect in substitutional alloys. Acta. Metall. **20**(3), 351–354 (1972). https://doi.org/10.1016/0001-6160(72)90028-4
S. Papanikolaou, Y. Cui, N. Ghoniem, Avalanches and plastic flow in crystal plasticity: An overview. Modell. Simul. Mater. Sci. Eng. **26**(1), 013001 (2018)
A. Portevin, F. Le Chatelier, Sur un phénomène observé lors de l'essai de traction d'alliages en cours de transformation. C. R. Acad. Sci. **176**, 507–510 (1923)
S. Rajesh, G. Ananthakrishna, Relaxation oscillations and negative strain rate sensitivity in the Portevin–Le Chatelier effect. Phys. Rev. E. **61**(4), 3664–3674 (2000)
N. Ranc, D. Wagner, Experimental study by pyrometry of Portevin-Le Châtelier plastic instabilities–Type A to type B transition. Mater. Sci. Eng. A. **474**(1-2), 188–196 (2008). https://doi.org/10.1016/j.msea.2007.04.012
S. Ren, M. Mazière, S. Forest, T. F. Morgeneyer, G. Rousselier, A constitutive model accounting for strain ageing effects on work-hardening. Application to a C–Mn steel. C. R. Mecanique. **345**(12), 908–921 (2017)
S. Ren, T. Morgeneyer, M. Mazière, S. Forest, G. Rousselier, Effect of Lüders and Portevin–Le Chatelier localization bands on plasticity and fracture of notched steel specimens studied by DIC and FE simulations. Int. J. Plast. **136**, 102880 (2021)
R. Shabadi, S. Kumar, H. J. Roven, E. S. Dwarakadasa, Characterisation of PLC band parameters using laser speckle technique. Mater. Sci. Eng. A. **364**(1-2), 140–150 (2004). https://doi.org/10.1016/j.msea.2003.08.013
R. Shabadi, S. Kumar, H. J. Roven, E. S. Dwarakadasa, Effect of specimen condition, orientation and alloy composition on PLC band parameters. Mater. Sci. Eng. A. **382**(1-2), 203–208 (2004). https://doi.org/10.1016/j.msea.2004.04.079
I. V. Shashkov, M. A. Lebyodkin, T. A. Lebedkina, Multiscale study of acoustic emission during smooth and jerky flow in an AlMg alloy. Acta Mater. **60**(19), 6842–6850 (2012). https://doi.org/10.1016/j.actamat.2012.08.058
W. Tong, H. Tao, N. Zhang, L. G. Hector, Time-resolved strain mapping measurements of individual Portevin-Le Chatelier deformation bands. Scr. Mater. **53**(1), 87–92 (2005). https://doi.org/10.1016/j.scriptamat.2005.03.020
A. Van den Beukel, Theory of the effect of dynamic strain aging on mechanical properties. Phys. Status Solidi A. **30**(1), 197–206 (1975)
E. Voce, The relationship between stress and strain for homogeneous deformation. J. Inst. Met. **74**, 537–562 (1948)
B. A. Wilcox, A. R. Rosenfield, On Serrated Yielding and Negative Strain-Rate Sensitivity. Mater. Sci. Eng. **1**(1), 201–205 (1966)
J. Xu, B. Holmedal, O. S. Hopperstad, T. Manik, K. Marthinsen, Dynamic strain ageing in an AlMg alloy at different strain rates and temperatures: experiments and constitutive modelling. Int. J. Plast. **151**, 103215 (2022)
M. Zaiser, Scale invariance in plastic flow of crystalline solids. Adv. Phys. **55**(1-2), 185–245 (2006). https://doi.org/10.1080/00018730600583514
M. Zaiser, P. Hähner, Oscillatory modes of plastic deformation: theoretical concepts. Phys. Status Solidi B. **199**(2), 267–330 (1997)
S. Zhang, P. G. McCormick, Y. Estrin, The morphology of Portevin-Le Chatelier bands: Finite element simulation for Al-Mg-Si. Acta Mater. **49**(6), 1087–1094 (2001). https://doi.org/10.1016/S1359-6454(00)00380-3

Y. Zhao, L. Dezerald, M. Pozuelo, X. Zhou, J. Marian, Simulating the mechanisms of serrated flow in interstitial alloys with atomic resolution over diffusive timescales. Nat. Commun. **11**(1), 1–8 (2020)
A. Ziegenbein, P. Hähner, H. Neuhäuser, Correlation of temporal instabilities and spatial localization during Portevin-Le Chatelier deformation of Cu-10 at.% Al and Cu-15 at.% Al. Comp. Mater. Sci. **19**(1-4), 27–34 (2000). https://doi.org/10.1016/S0927-0256(00)00136-1

Publisher's Note